Carrier diffusion in low-dimensional semiconductors: A comparison of quantum wells, disordered quantum wells, and quantum dots

A. Fiore,* M. Rossetti, B. Alloing, C. Paranthoen,† and J. X. Chen‡
Institute of Photonics and Quantum Electronics, Ecole Polytechnique, Fédérale de Lausanne, CH-1015 Lausanne, Switzerland

L. Geelhaar and H. Riechert
Infineon Technologies, Corporate Research Photonics, D-81730 München, Germany
(Received 13 May 2004; published 9 November 2004)

We present a comparative study of carrier diffusion in semiconductor heterostructures with different dimensionality [InGaAs quantum wells (QWs), InAs quantum dots (QDs), and disordered InGaNAs QWs (DQWs)]. In order to evaluate the diffusion length in the active region of device structures, we introduce a method based on the measurement of the current-voltage and light-current characteristics in light-emitting diodes where current is injected in an area $<1\ \mu m^2$. By analyzing the scaling behavior of devices with different sizes, we deduce the effective active area, and thus the diffusion length. A strong reduction in the diffusion length is observed going from QWs ($L_d \approx 2.7\ \mu m$) to QDs ($L_d < 100$ nm), DQWs being an intermediate case ($L_{diff} \approx 0-200$ nm depending on the carrier density). These results show that lateral composition fluctuations, either intended or unintended, produce strong carrier localization and significantly affect the carrier profile in a device even at room temperature.

DOI: 10.1103/PhysRevB.70.205311 PACS number(s): 73.63.Kv, 72.20.Ee, 72.80.Ng, 78.67.Hc

I. INTRODUCTION

Carrier diffusion plays an important role in the understanding and optimization of semiconductor optoelectronic devices, particularly lasers and light-emitting diodes. In the most common situation of two-dimensional (2D) heteroepitaxial growth, the potential profile and hence carrier transport, can be easily tailored in the growth direction, while in the layers plane transport is determined by diffusion. The diffusion length then sets the ultimate limit on the active device diameter. For example, the lowest threshold currents in quantum well (QW) vertical-cavity surface emitting lasers (VCSELs) are obtained in $2-3\ \mu m$ diameter devices, largely due to the loss of carriers due to the lateral diffusion in the QW for smaller diameters. For this reason, a large effort has been dedicated to the study and fabrication of active regions having a smaller diffusion length.[1–3] Diffusion processes strongly depend on the dimensionality of the active region: While 3D carrier diffusion is possible in a bulk unconfined active region, diffusion is restricted in a plane for a 2D quantum well, to a single direction for a quantum wire, and finally carriers are completely localized in an ideal 0D quantum dot (QD). Suppressed carrier diffusion in quantum dots has been indirectly evidenced in device characteristics such as the reduced sensitivity to defects,[4] better scaling of laser performance,[3] increased resistance to radiation damage,[5,6] and improved performance of ultrasmall devices.[7–9] Disordered QWs (DQWs) are an intermediate case between the 2D and 0D situations. In these structures, the essentially two-dimensional potential profile contains random fluctuation due, e.g., to inhomogeneities in the thickness or the composition of the QW (note that, in this context, the term "disordered" does not refer to the crystal quality of the QW). Thus, carriers can be localized in the minima of the potential profile, where they do not contribute to drift or diffusion. As the temperature or the injection level is increased, more and more carriers are promoted into higher-lying, unconfined energy states. In an energy band picture, the presence of disorder produces band tails corresponding to the localized states. Even in unconfined energy states within the band, the carrier mobility and the diffusion length are strongly reduced by scattering due to spatial inhomogeneities, as evidenced, e.g., in the AlGaN and InGaNAs material systems.[10,11]

Due to its fundamental and practical relevance, carrier diffusion has been experimentally investigated using a variety of techniques. In most cases, the ambipolar or unipolar diffusion length is measured on specifically designed structures by relatively sophisticated techniques, such as cathodoluminescence,[12] the transient-grating method,[13] or the high-resolution time-of-flight technique.[14] However, the measurement of the diffusion length in a device structure under working conditions would be preferred for the understanding and optimization of device characteristics. This has been demonstrated in edge-emitting lasers by fitting the subthreshold electrical impedance and modulation response[15] or the threshold current dependence on the stripe width.[3] These methods rely on specific laser models and require additional assumptions (e.g., the shape of the gain-current curve). Moreover, it is difficult to identify the process that is responsible for the broadening of the carrier profile, i.e., carrier diffusion in the active region versus current spreading in the injectors. Recently, we introduced[9] a fabrication technique that allows the realization of light-emitting diodes (LEDs) with dimensions comparable to the diffusion length (i.e., $<1\ \mu m$). The characteristics of such ultrasmall devices are very sensitive to diffusion and spreading processes. In this paper, we show that through a simple analysis of their current-voltage and light-current characteristics it is possible

to distinguish between current spreading and carrier diffusion, and to evaluate the diffusion length. This allows us to perform a comprehensive comparison of the diffusion process in QDs, QWs, and DQWs, as a function of the carrier density. In Sec. II, the device structure and fabrication are described, and the role of current spreading is analyzed. In Sec. III we present a comparative study of the diffusion length in similar structures comprising three different active regions, i.e., an InGaAs/GaAs QW, InAs/GaAs QDs, and a disordered InGaNAs QW. A diffusion length $L_d \approx 2.7$ μm is deduced for the InGaAs QW, while carrier localization ($L_d < 200$ nm) is observed in both the QDs and the InGaNAs DQW. In the DQW, we further show that the diffusion length increases with increasing current density, an indication of the filling of localized states in the band tail. The results are discussed in Sec. IV.

II. SAMPLE STRUCTURE AND FABRICATION

Three LED wafers were grown with very similar epitaxial structure except for the active regions. The samples (Fig. 1) were grown by molecular-beam epitaxy (MBE) on *n*-doped (001) GaAs substrates and consist of bottom-emitting microcavity LEDs with a bottom epitaxial distributed Bragg reflector (DBR) and a gold layer on the top, which serves both as a mirror and as a contact. The QD and QW samples were grown in the same VG-V80H MBE system and have an identical layer sequence: (from the bottom) 3.5-pairs *n*-doped GaAs/$Al_{0.9}Ga_{0.1}As$ quarter-wave stack (with 10 nm-thick graded layers at the interfaces), 20 nm *n*-$Al_{0.3}Ga_{0.7}As$, 114 nm *n*-GaAs, 45 nm undoped GaAs, an active layer (QDs or InGaAs QW), 45 nm undoped GaAs, 32 nm undoped AlGaAs with Al composition linearly increasing from 0% to 85%, 20 nm undoped $Al_{0.85}Ga_{0.15}As$, 115 nm *p*-$Al_{0.85}Ga_{0.15}As$, 10 nm graded layer, and a top p++ GaAs capping layer. Both *n*- and *p*-doping is nominally 2×10^{18} cm^{-3}, except in the capping layer, which is *p*-doped to 5×10^{19} cm^{-3}. The active layer consists in one sample of a 7.5 nm $In_{0.18}Ga_{0.82}As$ QW emitting at 980 nm at room temperature (RT), in the other sample of a self-assembled QD layer obtained by continuously depositing 2.9 monolayers of InAs and covering with a 5 nm-thick $In_{0.15}Ga_{0.85}As$ layer (RT emission around 1300 nm). The weak microcavity defined by the top Au mirror and the bottom 3.5 pairs Bragg mirror (quality factor $Q=20$) in this structure was designed to maximize the extraction efficiency for low-temperature emission at 1220 nm, therefore it is not optimized for the QD and QW RT emission wavelengths. The extraction efficiency, calculated by the dipole source-term method,[16] is 1.6% for the QW and 3.9% for the QD sample, at their respective emission wavelengths. The third DQW sample was grown in a different VG-V80H MBE apparatus and has the same layer sequence in the *p*-side of the junction and an active region composed of a 6.5 nm $In_{0.3}Ga_{0.7}N_{0.016}As_{0.984}$ QW sandwiched between two 5 nm $GaAs_{0.986}N_{0.014}$ barriers. The bottom DBR was replaced in this case by a $\lambda/2$-thick *n*-$Al_{0.3}Ga_{0.7}As$ layer. The InGaNAs QW emits at 1280 nm at RT and the calculated extraction efficiency at this wavelength is 8.3%. We stress that the InGaNAs sample was not annealed, in order to clearly evidence the compositional inhomogeneities in the DQW. While the *n*-side of the junction in this sample is different, it will be shown in the following that the light-current-voltage characteristics are determined by the *p*-injector, which is identical in the three structures, therefore a significant comparison can be made.

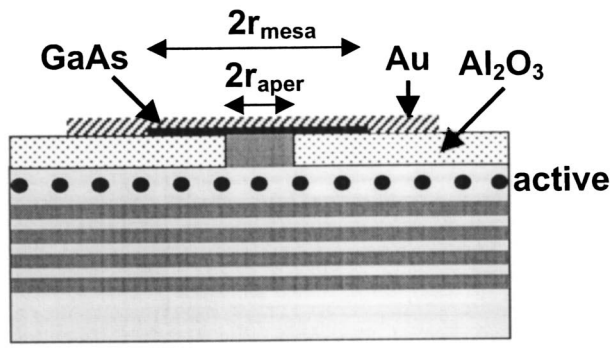

(a)

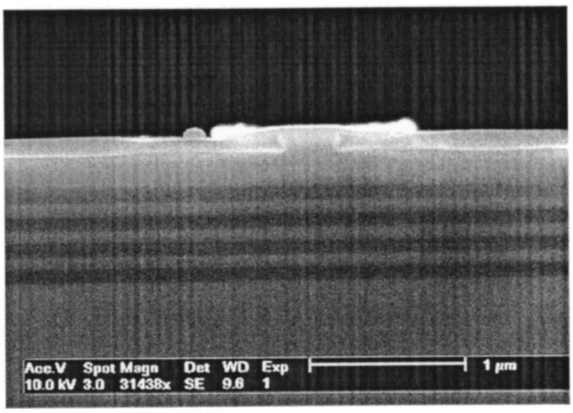

(b)

FIG. 1. (a) Schematics of the fabricated LED structures. (b) Cross-sectional SEM image of a 300-nm aperture obtained by lateral oxidation from a 1 μm-wide stripe.

LEDs with submicrometer current apertures were fabricated using the approach described in Ref. 9 and represented in Fig. 1. Device processing starts with the definition of shallow mesas of variable diameter (1–30 μm) by optical lithography and wet etching of the top GaAs cap layer. The exposed $Al_{0.85}Ga_{0.15}As$ is then oxidized selectively by heating the samples at 400 °C in a H_2O atmosphere created by bubbling N_2 in a water bath at 85 °C. The oxidation starts at the exposed surface and then penetrates laterally by $l_{ox} \approx 500$ nm under the GaAs cap layer, thus defining a current aperture whose diameter can be controlled down to around 100 nm by varying the oxidation time. Figure 1(b) shows a cross-sectional scanning-electron microscope (SEM) image of an aperture of 300 nm defined in this way. Broad area

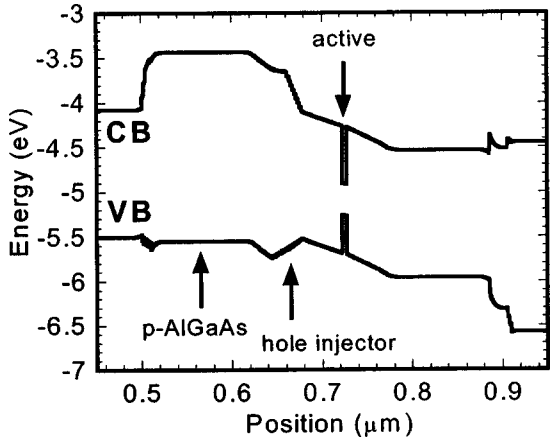

FIG. 2. Band diagram (CB: conduction band; VB: valence band) around the active region of the QD and QW LEDs under an applied bias of 1 V, calculated by Simwindows (Ref. 17), assuming a 5 nm-thick InAs QW as the active layer. The 32 nm-thick AlGaAs with Al composition linearly graded from 0% to 85% acts as a hole injector by accelerating holes toward the active layer.

p-contacts (3.8×10^{-5} cm^2) are then evaporated on top of the mesas, with uncritical alignment, and an *n*-contact is evaporated on the substrate side.

Because the surface of the sample, outside the mesas, is covered with an insulating Al_2O_3 oxide, current is forced to flow into the small current apertures. However, the active area may be larger than the current aperture if current spreads between the oxide aperture and the active layer. Current spreading must thus be suppressed to achieve a small active area. Current spreading is determined by the ratio of the lateral and vertical impedance: Particularly at low bias, when the diode impedance is large, current can find a lower impedance path by flowing laterally (parallel to the layers) and spreading on a much larger area. To suppress current spreading, the layers between the oxide aperture and the active layer were not doped in order to increase the lateral resistance.

Figure 2 shows the band diagram around the active region under an applied bias of 1 V, calculated by the Simwindows simulation package,[17] assuming a 5 nm-thick InAs QW as the active layer. Under a positive bias, the graded hole injector facilitates the vertical hole transport from the $Al_{0.85}Ga_{0.15}As$ aperture region to the QDs by avoiding potential steps at heterointerfaces in the valence band and by providing a potential gradient directed toward the active layer.

The role of current spreading and injector design was directly verified by comparing the current-voltage characteristics of two QD samples, one with the design described above, and a second one where the 32 nm-thick undoped graded injector and the 20 nm-thick undoped $Al_{0.85}Ga_{0.15}As$ were replaced by a 20 nm-thick *p*-doped $Al_{0.3}Ga_{0.7}As$ layer, which acts as a current-spreading layer. Broad-area LEDs with diameters ranging from 50 to 400 μm were fabricated using wet oxidation as described above. The current density *J* versus voltage *V* characteristics for (a) *p*-doped and (b) undoped graded injector structures are shown in Fig. 3 for different device diameters. All measurements shown in the following were taken in the two-probe configuration, in order to measure very small currents at low bias [the series resistance of the set-up ($\approx5\ \Omega$) contributes significantly to the measured voltage only for currents >10 mA, i.e., in the saturation region of the largest devices]. The current density was derived from the current using the measured current-aperture area. A strong difference between the two sets of curves is evident. The LEDs with optimized graded undoped injector show exponential diode characteristics (with ideality factor $n=1.8$), with nearly perfect scaling of current with aperture area: The current density versus voltage curves superpose over four orders of magnitude of current in the low bias range (for $V\geqslant0.8$ V the current becomes limited by the series and contact resistance, leading to a departure from exponential characteristics). In contrast, the LED with the current-spreading layer has strongly nonexponential *I-V* characteristics and does not show proper scaling with current aperture area. The absence of scaling is related to the fact that the effective device area is larger than the current aperture, which may be due to current spreading and/or to carrier diffusion. The nonexponential behavior of *I-V* characteristics

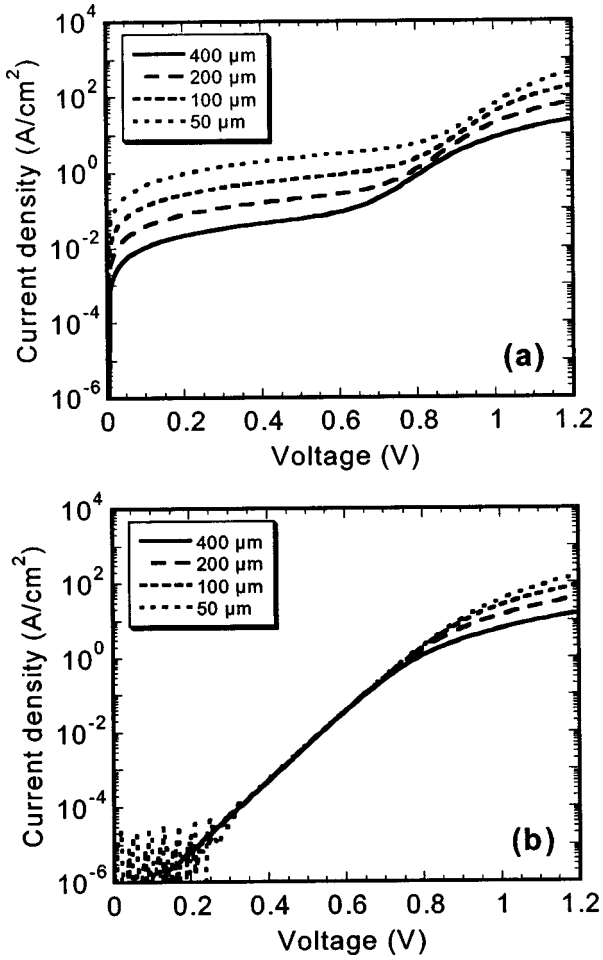

FIG. 3. Measured *J-V* characteristics of (a) QD LEDs with a doped current spreading layer, and (b) QD LEDs with an optimized injection region. The current density is obtained by dividing the current by the oxide aperture area.

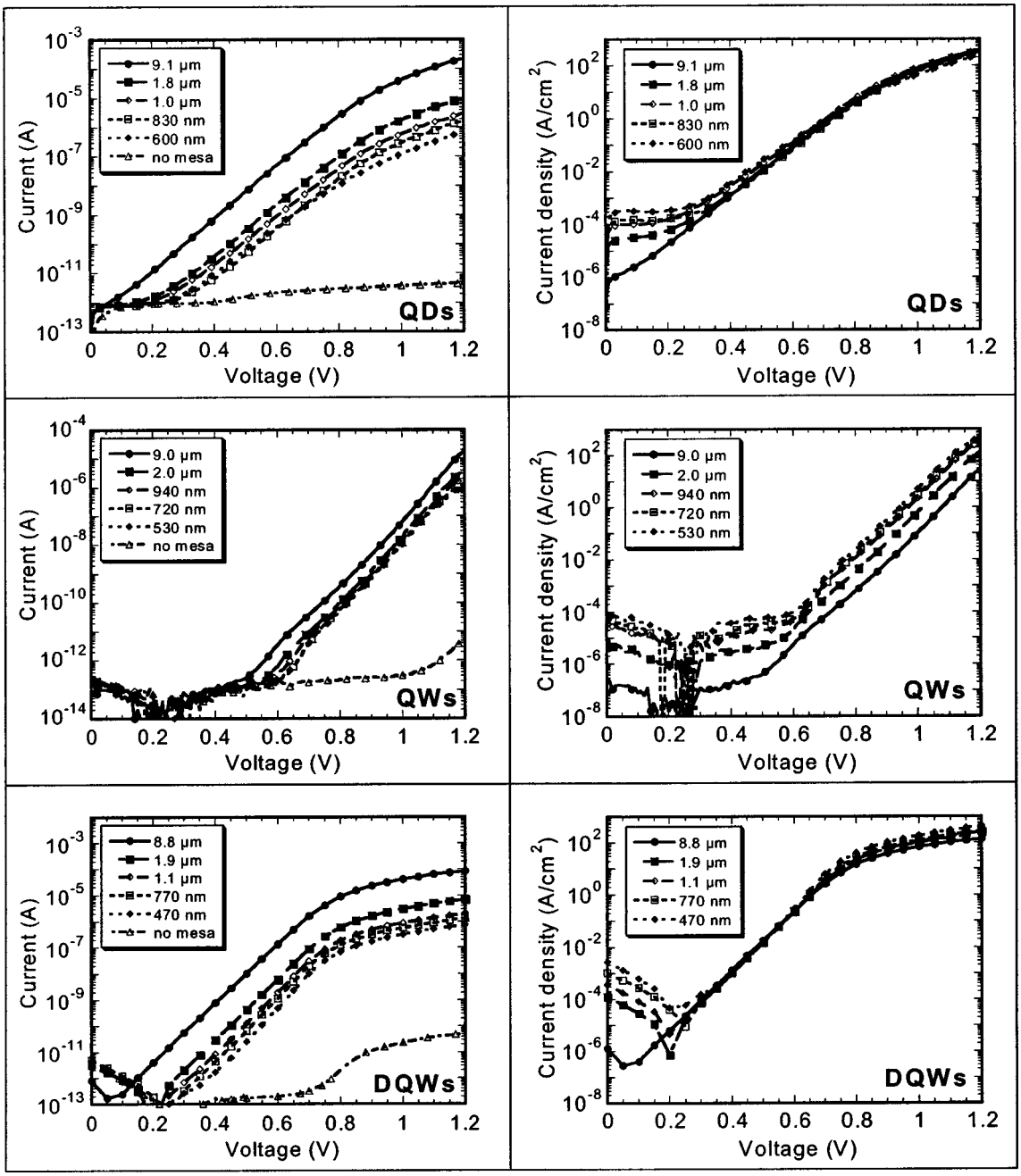

FIG. 4. Measured *I-V* (left) and *J-V* (right) characteristics for QD (top), QW (middle), and DQW (bottom) LEDs with different current-aperture diameters. The current densities are calculated using the aperture diameter measured by SEM during the process.

is strong evidence of current spreading, since this latter mechanism depends on the ratio of lateral to vertical impedance. Particularly, as the bias is reduced and thus the diode impedance increases, lateral current flow becomes more significant and the effective device area increases, leading to a higher current than in the undoped injector structure. In contrast, carrier diffusion does not depend on bias level and produces a bias-independent increase in the active diameter (see Sec. III). The comparison of the doped versus undoped injector structures shows that the *p*-injector plays a major role in the current-voltage characteristics of LEDs and lasers, and must be carefully optimized in order to avoid current spreading.

III. EXPERIMENTAL RESULTS

A. Current-voltage measurements

Current-voltage characteristics were measured on LEDs with QD, QW, and DQW active regions, for device diameters ranging from 10 μm to 500 nm and are reported in the left part of Fig. 4. All measurements were performed in the dark at room temperature. Control devices ("no mesa"), which were uniformly etched and thus have no aperture in the oxide layer, present only a very small leakage current through the oxide ($I<0.1$ nA at 1.2 V, corresponding to a current density $<3\times10^{-6}$ A/cm^2), which confirms that the oxide is effective in restricting current flow to the aperture

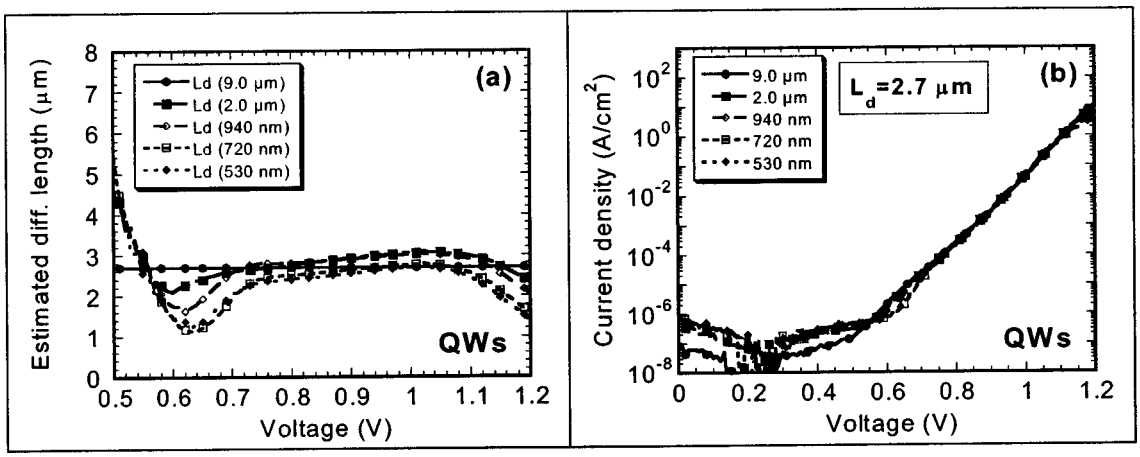

FIG. 5. (a) Estimated diffusion lengths in QW LEDs calculated from the ratio of current in each device to the current density in the 9 μm-diameter device (see the text). (b) Current densities versus voltage, assuming $L_d = 2.7$ μm.

region. The *I-V* curves present exponential diode characteristics over several orders of magnitude in the current, limited on the low bias side by the setup current sensitivity and on the high bias side by the series resistance due to space-charge-limited transport in the undoped AlGaAs layers and the contact resistance. In fact, in the high bias range ($V > 0.9$ V in the QD and DQW samples) the current has a square-law dependence on the voltage, which is typical for space-charge-limited transport.[18] The ideality factors, obtained by fitting the exponential part of the *I-V* characteristics of the largest devices, are $n = 1.89$ (QD), 1.54 (QW), and 1.53 (DQW). Note that, because of the smaller bandgap of the active region, a higher current is observed in the QD and DQW samples than in the QW. Persistent photoconductivity due to ambient illumination was observed in the QW and DQW LEDs, leading to negative currents at low bias ($V < 0.2$ V) (this corresponds to the discharge of photocreated carriers, which is slow due to the extremely high diode impedance). In order to alleviate this effect, the voltage was swept from 0 to 1.4 V several times before taking each measurement. Note that in the QD structures the same effect is not observed because of the much reduced absorption in the active region.

For each device size, the diameter of the current aperture was measured by SEM during the process and used in the calculation of the current density (the right part of Fig. 4). Comparing the current density for different device diameters, we observe a different scaling behavior depending on the nature of the active region. For the QD structures, the current density versus voltage characteristics do not depend on the device size over four orders of magnitude in the current density, i.e., in the bias range $0.4\ \text{V} \leqslant V \leqslant 0.9$ V corresponding to exponential diode characteristics. The good scaling basically confirms that current spreading and carrier diffusion are insignificant, as already observed from the characteristics shown in Fig. 3, except that, due to the much smaller sizes, we can now put a much more stringent upper limit on the diffusion length. If, e.g., a diffusion/spreading length of 100 nm is added to the device radius measured by SEM, the curves show a significant departure from the scaling behavior shown in Fig. 4. This sets an upper limit of $\approx$100 nm on the diffusion *and* spreading lengths in our QD devices. This resolution in the determination of the active device area results directly from the use of submicrometer current apertures, a unique feature of our approach.

In contrast to the QD structures, the QW LED current-voltage characteristics do not scale with the current aperture area: Smaller devices have an apparently higher current density. This is due to the fact that the active area is increased by the diffusion of carriers along the laterally uniform QW. In fact, since the epitaxial structure of the QW LED is identical to the QD LED, apart from the active region, we can rule out current spreading in the injection region as the origin for the increased active area. This is further confirmed by the nicely exponential *I-V* characteristics of the QW sample, different from the current-spreading behavior shown in Fig. 3(a). Based on this observation, we can deduce the diffusion length from the scaling of *I-V* characteristics with device area. Specifically, we expect the active radius to be given by the radius of the unoxidized region increased by a diffusion length L_d, which should not depend on the device size and bias point. The current for device n is then given by

$$I_n(V) = J_0(V) S_n = J_0(V) \pi (r_{\text{aper},n} + L_d)^2, \qquad (1)$$

where S_n is the effective active area, $r_{\text{aper},n}$ is the aperture radius, and J_0 is the current density in a planar device (i.e., for the case where L_d is negligible compared to the aperture radius). As a starting point, we take J_0 as the current density calculated from the largest (9 μm-diameter) device using the current aperture area. For each device, we calculate $L_d = L_d(V)$ from Eq. (1). We find that, in the voltage range 0.7–1.1 V, where the *I-V* characteristics are exponential, L_d has a value approximately independent of the voltage. The procedure is then iterated by using this value in the calculation of J_0, until a self-consistent value of L_d is found. Figure 5(a) shows the $L_d(V)$ curves, obtained assuming $L_d = 2.7$ μm in the calculation of J_0 from the current of the 9 μm-diameter device. Remarkably, $L_d(V) = (2.7 \pm 0.4)$ μm in a voltage range that corresponds to over four orders of magnitude of current density variation and for devices whose diameters span two orders of magnitude. The scaling of $J(V)$

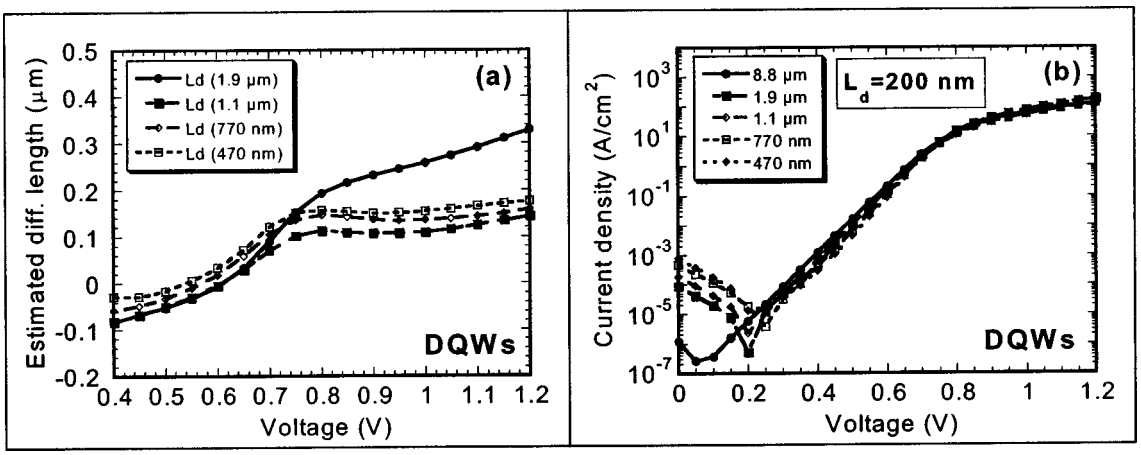

FIG. 6. (a) Estimated diffusion lengths in DQW LEDs calculated from the ratio of current in each device to the current density in the 8.8 μm- diameter devices (see the text). (b) Current densities versus voltage, assuming L_d=200 nm.

characteristics obtained by assuming L_d=2.7 μm is shown in Fig. 5(b) and further demonstrates the accuracy of the fit. We stress that the possibility of fitting the $J(V)$ curves with a single parameter confirms that the diffusion process depends on the active material and not on the device size and the applied voltage.

Finally, the DQW LED characteristics scale relatively well with the current aperture area, as seen in Fig. 4 (bottom right). However, at high bias ($V>0.7$ V) smaller devices present an apparently larger current density—an indication for carrier diffusion. We apply the same procedure as for the QW LEDs, taking J_0 as the current density calculated from the 8.8 μm-diameter device using the current aperture area. The diffusion lengths calculated using Eq. (1) are shown in Fig. 6(a). In this case, L_d is negligible (within the resolution of $\approx$100 nm due to dispersion in the characteristics of the different devices) for $V<0.6$ V, however, for higher bias it clearly increases with bias with a saturation in the 150–200 nm range. This trend is observed in all the devices and the diffusion lengths are comparable. Note that the relative variation of L_d in the DQWs is much larger than in QWs, where it is below 20% in a comparable bias range. We attribute the increase of diffusion length to a progressive filling of localized states in the band tail of the disordered GaInNAs QWs and consequent population of delocalized states in the band, as discussed in Sec. IV. Figure 6(b) reports the *J-V* characteristics obtained by taking into account a diffusion length L_d=200 nm in the calculation of the active area. The scaling is better in the high bias part of the characteristics, as expected.

B. Light-current measurements

Light-current measurements were taken using a calibrated Ge detector with an active area of 1 cm^2 positioned close ($\approx$1 mm) to the sample backside, in order to collect most of the optical power emitted by the LEDs. Lock-in techniques are used to accurately measure the low-power levels produced by these small devices. Figure 7 (left side) shows the power P versus current I characteristics measured on the QD (top), QW (middle), and DQW (bottom) LEDs. The external quantum efficiency η_{QE}, calculated as $\eta_{QE}=(e/h\nu)/(P/I)$, is plotted in the right part of Fig. 7 as a function of the *nominal* current density (current divided by the aperture area).

The light-current characteristics on the QD LEDs show that at low current levels smaller devices are more efficient. This effect is mostly due to the fact that at low bias efficiency increases with current density (reaching a maximum around 100 A/cm^2; see the right part of Fig. 7), and that for a given current smaller devices operate at higher current densities, thus closer to the optimum point. This is a clear demonstration that proper size scaling is needed in order to achieve efficient light generation at low output power levels. At higher bias, on the contrary, the output power from smaller devices saturates due to the filling of the QD ground state level and population of excited states, which are more prone to nonradiative recombination due to thermal escape. In order to de-embed the material properties from the effect of the microcavity, the external quantum efficiency can be written as $\eta_{\mathrm{QE}}=\eta_{\mathrm{rad}}\,\eta_{\mathrm{extr}}$, where η_{rad} is the radiative efficiency (the number of photons generated inside the device divided by the number of injected electrons) and η_{extr} is the extraction efficiency (the fraction of internally generated photons that escape to the outside). By dividing the measured external quantum efficiency by the extraction efficiency η_{extr}=3.9%, calculated by the dipole source-term method,[16] we deduce the radiative efficiency as a function of current density, plotted in Fig. 8 (top). The radiative efficiency versus current density curves scale well with each other, except for the two largest diameters, which present a lower peak efficiency. Also, the efficiency was observed to vary considerably among nominally identical devices for the smallest diameters in this sample (the best values are presented). Variation in the efficiency related to the increase in the spontaneous emission rate in the cavity mode (the so-called Purcell effect[19,20]) can be excluded, despite the small active areas, since the cavity quality factor is too small in this structure. We rather attribute the scattering and reduced efficiency for the large devices to the presence of defects with areal density such that one or a few may be present in each LED. The presence of defects is also confirmed by the relatively low peak radiative efficiency of 2.5% measured in

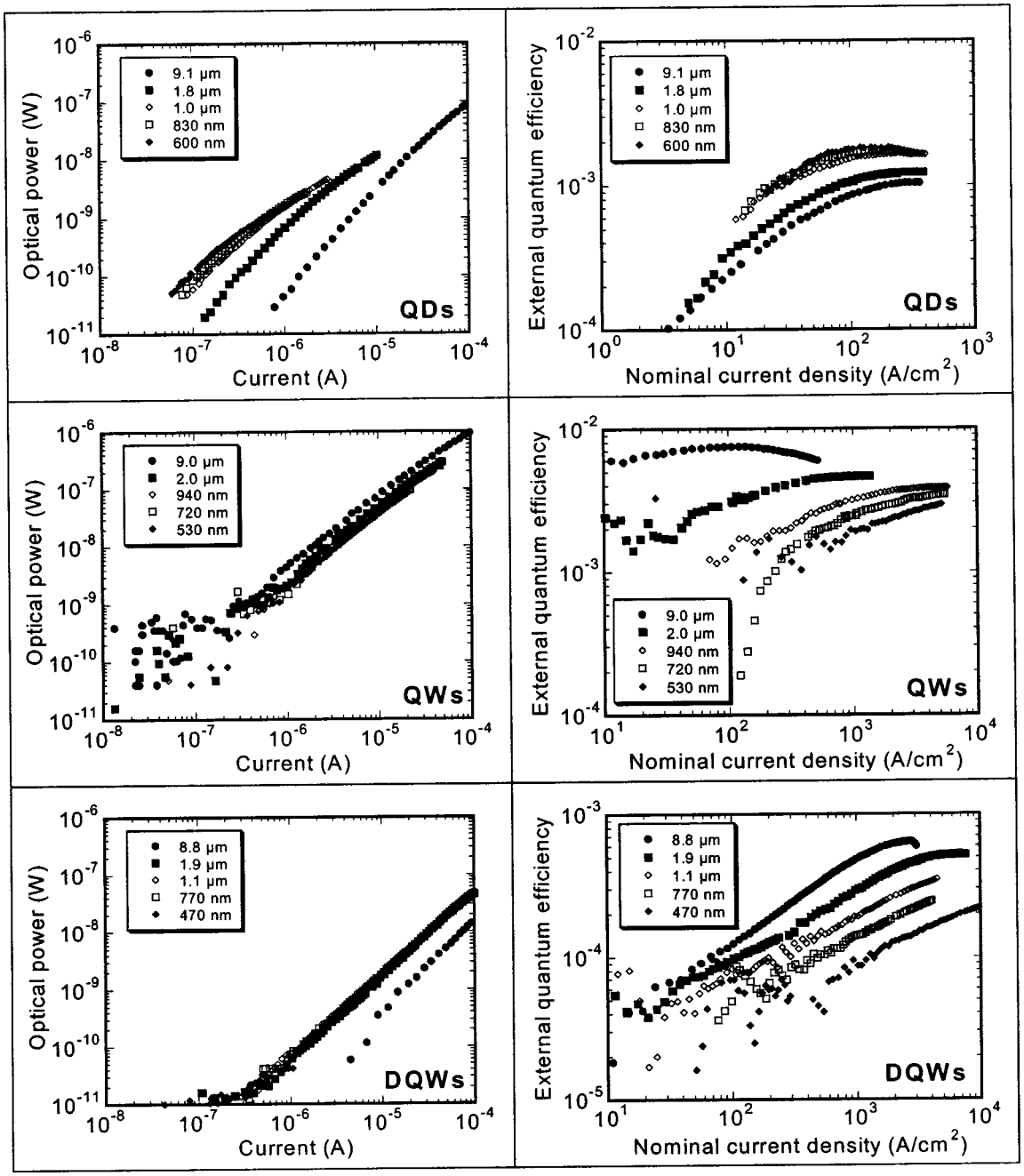

FIG. 7. Measured power-current (left) and efficiency-current density (right) characteristics for QD (top), QW (middle), and DQW (bottom) LEDs with different current-aperture diameters. The nominal current densities are calculated using the aperture diameter measured by SEM.

large (400 μm) devices, even with no oxide aperturing, as compared to the radiative efficiencies of 13% measured by us[21] in similar QD structures. The main conclusion is that the efficiency is not degraded even for the smallest areas, which indicates that the oxide layer does not introduce nonradiative recombination centers in the QD layer along the perimeter of the aperture, which would become more significant as the device shrinks in size. Also, all devices reach the peak efficiency at similar current density levels, further confirming that proper size scaling is achieved in QD LEDs.

This situation should be contrasted with the efficiency versus current density curves for QW LEDs (Fig. 7, middle part), where (a) the peak efficiency decreases as the device diameter is reduced, and (b) the optimum current density increases by over one order of magnitude as the diameter is decreased from 9 to 0.5 μm. The latter effect is clearly related to the increase in the effective active area due to carrier diffusion in the QW, as observed in the current-voltage characteristics. By using the effective current densities (assuming L_d=2.7 μm) we easily recover efficiency curves which have the same functional dependence on the current densities (not shown). However, in order to explain the variation in the peak quantum efficiencies, we must introduce one further element: The extraction efficiency depends on whether re-

combination occurs in the aperture area, in the annular region below the mesa and the oxide [see Fig. 1(a)], or in the etched area outside the mesa. The output power can in fact be written as

$$P_{\text{out}} = \frac{h\nu}{e}\eta_{\text{rad}}(\eta_{\text{aper}}I_{\text{aper}} + \eta_{\text{ox}}I_{\text{ox}} + \eta_{\text{etch}}I_{\text{etch}}) = \frac{h\nu}{e}\eta_{\text{rad}}\left(\eta_{\text{aper}}\frac{S_{\text{aper}}}{S_{\text{tot}}} + \eta_{\text{ox}}\frac{S_{\text{ox}}}{S_{\text{tot}}} + \eta_{\text{etch}}\frac{S_{\text{etch}}}{S_{\text{tot}}}\right)I, \quad (2)$$

where η_{aper}, η_{ox}, and η_{etch} are the extraction efficiencies for photons generated in the aperture, oxidized, and etched regions, respectively, I_{aper}, I_{ox}, and I_{ctch} the currents in the three regions, S_{aper}, S_{ox} and S_{etch} the corresponding areas ($S_{\text{aper}}=\pi r_{\text{aper}}^2$, $S_{\text{ox}}=\pi(r_{\text{mesa}}^2-r_{\text{aper}}^2)$, and $S_{\text{etch}}=\pi[(r_{\text{aper}}+L_d)^2 - r_{\text{mesa}}^2]$, where r_{aper} and r_{mesa} are the radii of the oxidized aperture and of the etched mesa, respectively), S_{tot} the total effective active area **(**$S_{\text{tot}}=\pi(r_{\text{aper}}+L_{\text{d}})^2$**)**, $h\nu$ the photon energy, and e the electron charge. In (2) we have assumed the current density to be uniform in the active area, which is the same approximation used in the fitting of L_d from the current-voltage characteristics. Note that we are not considering any surface recombination effect, which is consistent with the good scaling of *L-I* characteristics observed in the QD sample. By using a simulation software based on the dipole source-term method,[16] we calculate the extraction efficiency as (at $\lambda=970$ nm): $\eta_{\text{aper}}=1.6\%$ in the aperture region, $\eta_{\text{ox}}=1.9\%$ below the oxide, and $\eta_{\text{etch}}=0.495\%$ in the etched area. Using these values, the measured geometrical areas and the diffusion length $L_d=2.7$ μm derived from the current-voltage characteristics, the radiative efficiency η_{rad} can be calculated from (2) for different device diameters and bias conditions. The result is plotted in Fig. 8 (middle part) as a function of the *effective* current density $J_{\text{eff}}=I/S_{\text{tot}}$. The scaling between the different curves is very good (apart from some discrepancy for the largest device at low current densities), despite the simplicity of the model and the absence of fitting parameters (apart from the diffusion length that was fitted separately from the *I-V* characteristics). This confirms that the decrease in efficiency for the small QW LEDs, as seen in Fig. 7, is only due to the diffusion of carriers outside the aperture area, and not to defects introduced by the oxide.

The DQW efficiency versus current densities (Fig. 7, bottom part) also show considerable dispersion for different diameters, despite the smaller carrier diffusion evidenced by the current density versus voltage measurements. In particular, similarly to the QW LEDs, the smaller devices present both a lower peak external quantum efficiency and an increased optimum current density, which is an indication for carrier diffusion outside of the aperture area. We note that the light-current measurements were taken at relatively high current densities ($J>10$ A/cm^2), since the radiative efficiency of InGaNAs is very low at low carrier concentration, due to nonradiative recombination, as shown previously.[22,23] In this range, we estimated L_d to be in the order of 200 nm from the scaling of current-voltage characteristics [Fig. 6(a)]. In order to check this estimate, similarly to the QW LEDs, we write the extraction efficiency as the weighted sum of the efficiencies in the different regions. In this case, however, since L_d is smaller than the oxidized distance l_{ox}, we assume that carriers do not diffuse outside of the oxidized aperture, i.e., we neglect photon generation in the etched region, and thus

$$P_{\text{out}} = \frac{h\nu}{e}\eta_{\text{rad}}(\eta_{\text{aper}}I_{\text{aper}} + \eta_{\text{ox}}I_{\text{ox}}) = \frac{h\nu}{e}\eta_{\text{rad}}\left(\eta_{\text{aper}}\frac{S_{\text{aper}}}{S_{\text{tot}}} + \eta_{\text{ox}}\frac{S_{\text{ox}}}{S_{\text{tot}}}\right)I. \quad (3)$$

In this case, $S_{\text{aper}}=\pi r_{\text{aper}}^2$, $S_{\text{ox}}=\pi[(r_{\text{aper}}+L_d)^2-r_{\text{aper}}^2]$. The extraction efficiencies are calculated as $\eta_{\text{aper}}=8.3\%$ in the aperture region and $\eta_{\text{ox}}=0.75\%$ below the oxide, at the emission wavelength of 1280 nm (these are different from the QW sample because of the different emission wavelength and bottom mirror structure). The radiative efficiency is plotted in Fig. 8 (bottom part) as a function of the effective current density, assuming a diffusion length $L_d=200$ nm. The scaling of the different curves is now excellent and further supports the estimated value of L_d derived from the current-voltage characteristics. Note that the scaling analysis of the light-current characteristics provides additional information as compared to the current-voltage characteristics. In fact, the diffusion length impacts the light-current characteristics more strongly since it affects also the extraction efficiency, particularly in the smallest devices where the diffusion area may be comparable to the current aperture. Moreover, light-current investigations allow the measurement of the diffusion length in a current density range ($J>10^3$ A/cm^2) where the current-voltage characteristics are dominated by the voltage drop due to the series resistance and the space-charge-limited transport.

Finally, we compare the radiative efficiency of the InGaAs QW emitting at 980 nm to InGaNAs DQW and InAs QDs, both emitting around 1300 nm, as shown in Fig. 8. The InGaAs QW has the highest radiative efficiency, approaching 70% at a current density of 30 A/cm^2, which is a typical value for high-quality InGaAs QWs. The QD LEDs present radiative efficiencies in the 3%–5% range, a somewhat lower value than the 13% previously measured by us[21] on similar epitaxial material. Carrier capture by strain-induced defects and reduced spontaneous emission rate due to thermal activation to the barriers and/or to excited states may be the origin of the lower radiative efficiency of QDs as compared to optimized QWs. InGaNAs QWs have an even lower radiative efficiency than QDs, as was previously observed through a direct comparison between the two materials.[22] This is likely due to nonradiative defects directly or indirectly related to *N* incorporation, which result in much shorter nonradiative lifetimes, particularly in this nonannealed material. Note also that the radiative efficiency maximum (possibly limited by device heating) corresponds to high current densities >1 kA/cm^2, further evidence of nonradiative recombination.

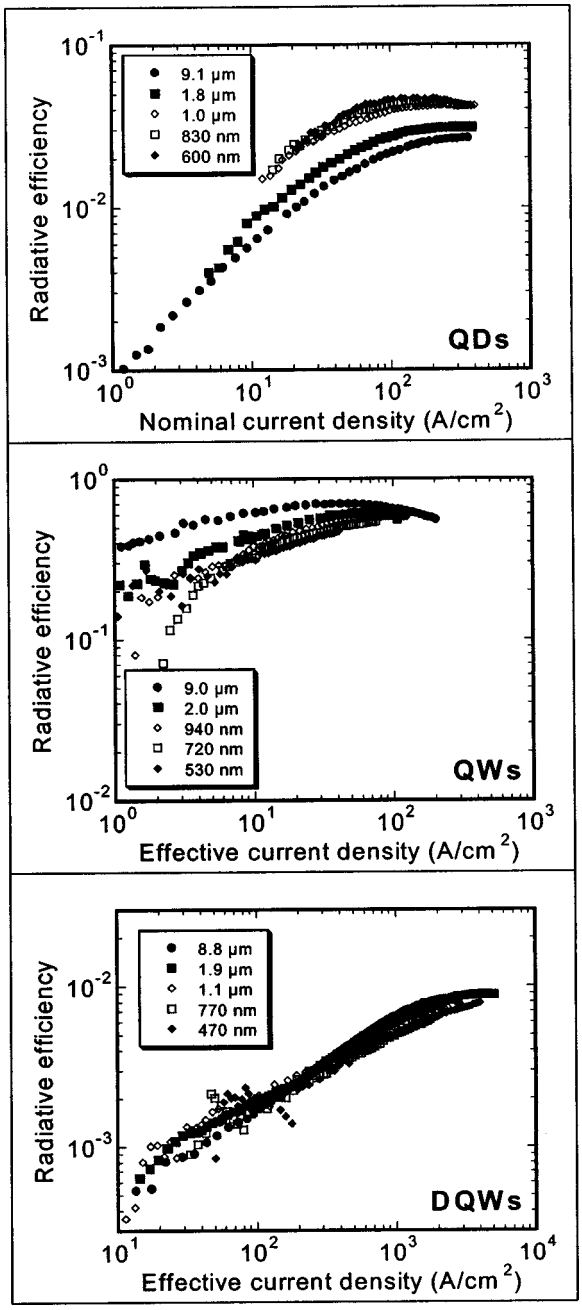

FIG. 8. Radiative efficiency versus current density characteristics for QD (top), QW (middle), and DQW (bottom) LEDs with different current-aperture diameters. The current densities are calculated assuming no diffusion for the QDs, a diffusion length $L_d = 2.7$ μm for the QWs and $L_d = 200$ nm for the DQWs.

IV. DISCUSSION

The set of measurements presented in Sec. III provides a consistent estimate of the diffusion lengths in semiconductor nanostructures of different dimensionality, i.e., QWs, QDs, and disordered QWs, as a function of the carrier concentration. The first issue that needs to be clarified is whether the measured value is the minority carrier or the ambipolar diffusion length. In fact, the diffusion mechanism depends on the type and geometry of carrier injection. Although no external field is applied in the lateral plane, an imbalance of electron and hole concentrations can produce an electric field that contributes to charge transport through a drift term. For example, in the case of optical excitation of carriers in an undoped semiconductor, the conditions of charge neutrality and zero total current density lead to ambipolar diffusion, where the transport including diffusion and drift can be described as a purely diffusive process with an ambipolar diffusion coefficient given, for a nondegenerate semiconductor, by

$$D_a = 2\frac{D_n D_p}{D_n + D_p} \tag{4}$$

(see, e.g., Ref. 24), where D_n and D_p are the electron and hole diffusion coefficient, respectively. However, as pointed out by Joyce,[25] the localized injection of holes from an aperture or a mesa does not correspond to the situation of ambipolar diffusion, since the supply of carriers is asymmetric (localized injection of holes from the p side, uniform injection of electrons from the n side). A similar derivation as in the case of ambipolar diffusion leads[25] to describing both transport and diffusion with an effective diffusion coefficient,

$$D_e \approx 2D_p. \tag{5}$$

It is seen that, although representing different physical situations, expressions (4) and (5) give approximately the same value of the diffusion coefficient in the case $D_n \gg D_p$ (note, however, that, if electrons were confined instead of holes, only the derivation by Joyce would correctly predict a much larger effective diffusion coefficient $D_e \approx 2D_n$). Intuitively, the internal electric field favors hole transport against electron transport, counteracting the difference in diffusion coefficients, in order to maintain charge neutrality. Assuming that the carrier lifetime τ is independent of the carrier concentration, the diffusion length $L_d \approx 2.7$ μm fitted from the I-V characteristics in our QW LEDs is related to the effective diffusion coefficient through

$$L_d = \sqrt{D_e \tau} \approx \sqrt{2D_p \tau}, \tag{6}$$

and is thus also approximately equal to the ambipolar diffusion length since electron mobilities are much larger than hole mobilities in InGaAs QWs. Note that the diffusion length is fitted over a low bias range ($J < 10$ A/cm^2), where the assumption of a constant lifetime is reasonable (monomolecular recombination).

The estimate of the QW ambipolar diffusion length obtained by our method, $L_d(V) = (2.7 \pm 0.4)$ μm, is within the range of values reported in the literature; see, e.g., Refs. 1, 12, 26, and 27. The significant spread in these values may be attributed, besides the material quality, to the different excitation levels used in the different experiments (a strong

reduction in L_d was, for example, observed in Ref. 27 with increasing current injection in a laser structure).

The suppression of carrier diffusion in QDs and disordered QWs, as compared to QWs, was also reported previously. Ambipolar diffusion length values of $L_d \approx 0.5$ μm ($In_{0.3}Ga_{0.7}As$ QDs emitting at 1180 nm[28]) and $L_d < 0.6$ μm (resolution limited, InAs QDs emitting at 1270 nm[29]) were measured in QDs using cathodoluminescence and spatially resolved photoluminescence, respectively. Our more stringent estimated upper limit $L_d < 100$ nm derives on one side from the stronger electronic confinement (as compared to the QDs used in Ref. 28), on the other side from the better spatial resolution (as compared to Ref. 29), which is provided by the small current apertures and the large dynamic range in *I-V* measurements. The strongly suppressed carrier diffusion in QDs is clearly related to 3D wave function confinement in the low-bandgap islands. The possible mechanisms for diffusion in QDs are (a) thermal hopping and (b) diffusion in the 2D wetting layer (WL) or the 3D GaAs barrier, prior to carrier capture in the QDs. For the large and In-rich QDs and at the low injection levels considered here, thermal hopping is ineffective due to the large potential barrier (270 meV) between the QD ground state exciton energy and the WL energy. The latter mechanism, diffusion prior to carrier capture, has been evoked in Ref. 29 to explain the comparatively larger diffusion length ($L_d \approx 1.6$ μm) measured when pumping in the GaAs barrier. In contrast, although injection proceeds through the barrier also in our LEDs, we do not observe such an effect. We attribute this difference to the different excitation density used in the two experiments. Indeed, diffusion prior to capture should be negligible in our dots, since the capture time from the barrier to the QDs is smaller than 10 ps[30]).

Finally, it is remarkable that diffusion is strongly suppressed ($L_d = 0-200$ nm, depending on carrier density) in InGaNAs DQWs at room temperature. The minority carrier diffusion length in bulk MBE-grown InGaNAs (after annealing) has been previously estimated by fitting the response characteristics of solar cells:[11] $L_d(\text{holes}) = 30$ nm. However, to the best of our knowledge, the ambipolar diffusion length in InGaNAs QWs has not been reported previously. The very short minority and ambipolar diffusion lengths can be attributed to short carrier lifetimes, to scattering by impurities and by spatial inhomogeneities, or to localized energy states in the band tail. Several of these factors are likely to contribute, depending on the carrier concentration and temperature. Particularly, the current-voltage measurements presented in Figs. 4 and 6 evidence an increase of the diffusion length at high carrier injection, which may indicate a transition from diffusion through hopping among localized states to bandlike transport. In fact, compositional disorder in an alloy produces a band tail consisting of states with localized wave functions. At low current densities holes occupy the localized states in the band tail, which are progressively filled as injection is increased, leading to the population of delocalized states inside the band and increased diffusion. Compositional fluctuations along InGaNAs QWs were observed by transmission electron microscopy.[31] Also, carrier localization at low temperature was indicated for such structures by an S-shape dependence of the photoluminescence (PL) peak position on temperature.[32,33] In bulk InGaNAs, evidence of exciton localization at low temperature was provided both by time-resolved PL[34] and by the appearance and magnetic-field dependence of sharp spectral lines in near-field spectroscopy.[35] While in most reports localization effects are significant for temperatures <100 K, our data indicate that they may persist up to room temperature in our nonannealed InGaNAs QWs. There are several effects that could cause this apparent difference: First, the compositional inhomogeneities giving rise to localization are more significant in nonannealed layers.[36–40] However, it should be noted that PL measurements on a nonannealed reference sample analogous to the DQW LED revealed a very weak S-like dependence of the peak position on temperature (localization depth about 5 meV, data not shown). Second, the carrier density may also be an important factor for the observation of localization effects: The transition between localized and bandlike behavior, as evidenced by the increase in the diffusion length, is observed at low current densities $J < 10$ A/cm^2, corresponding to carrier densities $<10^{10}$ cm^{-2}. This excitation range is usually not accessible in optical measurements, because nonradiative recombination is dominant, as we observe in the LED characteristics as well (Fig. 8). Two recent studies on carrier transport in (In)GaNAs layers have in fact evidenced localization effects at temperatures up to 200[41] and 300 K[42] at low carrier densities. More investigations specifically devoted to the InGaNAs material as such are needed to clarify this point.

V. CONCLUSIONS

The main results presented in this paper are two-fold. First, we have introduced a convenient method for characterizing the diffusion in device structures. The method is based on the analysis of the scaling behavior of light-emitting diodes, where carrier injection is confined within dimensions well below 1 μm. By a careful control of current spreading, we have indeed shown that the current-voltage and light-current characteristics are entirely determined by the diffusion of carriers in the active region, which allows the measurement of the diffusion length. Second, we have performed a comparative investigation of diffusion in semiconductor heterostructures having different dimensionality: quantum wells, quantum dots, and disordered quantum wells. Significant in-plane diffusion (diffusion length $L_d \approx 2.7$ μm) in high-quality InGaAs/GaAs quantum wells results in bad scaling in current-voltage (current does not scale with the device area) and light-current characteristics (efficiency decreases as the area is reduced). In contrast, in-plane compositional fluctuations in quantum dots and disordered quantum wells are effective in suppressing carrier diffusion ($L_d < 100$ nm in QDs and $L_d \leqslant 200$ nm in DQWs). The increase of the diffusion length with increasing carrier density in disordered QWs shows the filling of localized energy states in the band tail and the population of higher energy delocalized levels. Beside the fundamental interest in diffusion processes in semiconductor heterostructures, these

results show that the control of carrier diffusion, provided, e.g., by quantum dots, is essential to fabricate efficient devices (LEDs, lasers) with dimensions in the submicrometer scale. In particular, the possibility of injecting current in a submicrometer area is relevant for the realization of ultralow threshold lasers and efficient, single QD LEDs to be used as single-photon sources for quantum communication.

ACKNOWLEDGMENTS

We are grateful to Dr. R. P. Stanley (CSEM Neuchâtel) for many interesting discussions. Financial support from the European Commission through the 5th framework IST project "GSQ" and from the Swiss National Science Foundation is acknowledged.

*Permanent address: Institute of Photonics and Nanotechnology CNR-IFN, via del Cineto Romano 42, 00156 Roma, Italy; electronic address: andrea.fiore@epfl.ch

†Present address: Laboratoire d'étude des nanostructures semiconductrices (LENS), INSA, 20 av. des Buttes de Coësmes—35043 Rennes, France.

‡Present address: Bell Laboratories, Lucent Technologies Inc., 600 Mountain Ave., Murray Hill, New Jersey 07974, USA.

[1] T. A. Strand, B. J. Thibeault, and L. A. Coldren, J. Appl. Phys. **81**, 3377 (1997).

[2] R. L. Naone, P. D. Floyd, D. B. Young, E. R. Hegblom, T. A. Strand, and L. A. Coldren, IEEE J. Sel. Top. Quantum Electron. **4**, 706 (1998).

[3] J. K. Kim, R. L. Naone, and L. A. Coldren, IEEE J. Sel. Top. Quantum Electron. **6**, 504 (2000).

[4] J. M. Gérard, O. Cabrol, and B. Sermage, Appl. Phys. Lett. **68**, 3123 (1996).

[5] P. G. Piva, R. D. Goldberg, I. V. Mitchell, D. Labrie, R. Leon, S. Charbonneau, Z. R. Wasilewski, and S. Fafard, Appl. Phys. Lett. **77**, 624 (2000).

[6] C. Ribbat, R. Sellin, M. Grundmann, D. Bimberg, N. A. Sobolev, and M. C. Carmo, Electron. Lett. **37**, 174 (2001).

[7] M. Arzberger, G. Böhm, M.-C. Amann, and G. Abstreiter, Appl. Phys. Lett. **79**, 1766 (2001).

[8] K. J. Luo, J. Y. Xu, H. Cao, Y. Ma, S. H. Chang, S. T. Ho, and G. S. Solomon, Appl. Phys. Lett. **78**, 3397 (2001).

[9] A. Fiore, J. X. Chen, and M. Ilegems, Appl. Phys. Lett. **81**, 1756 (2002).

[10] K. C. Zeng, J. Y. Lin, and H. X. Jiang, Appl. Phys. Lett. **76**, 1728 (2000).

[11] S. R. Kurtz, J. F. Klem, A. A. Allerman, R. M. Sieg, C. H. Seager, and E. D. Jones, Appl. Phys. Lett. **80**, 1379 (2002).

[12] H. A. Zarem, P. C. Sercel, J. A. Lebens, L. E. Eng, A. Yariv, and K. J. Vahala, Appl. Phys. Lett. **55**, 1647 (1989).

[13] J. R. Salcedo, A. E. Siegman, D. D. Dlott, and M. D. Fayer, Phys. Rev. Lett. **41**, 131 (1978).

[14] H. Hillmer, A. Forchel, S. Hansmann, M. Morohashi, E. Lopez, H. P. Meier, and K. Ploog, Phys. Rev. B **39**, 10901 (1989).

[15] M. S. Torre, I. Esquivias, B. Romero, K. Czotscher, S. Weisser, J. D. Ralston, E. Larkins, W. Benz, and J. Rosenzweig, J. Appl. Phys. **81**, 6268 (1997).

[16] H. Benisty, R. P. Stanley, and M. Mayer, J. Opt. Soc. Am. A **15**, 1192 (1998).

[17] Simwindows, http://www-ocs.colorado.edu/SimWindows/simwin.html

[18] J. G. Simmons, "Electronic conduction through thin insulating films," in *Handbook of Thin Film Technology*, edited by L. I. Maissel and R. Glang (McGraw-Hill, New York, 1983).

[19] E. M. Purcell, Phys. Rev. **69**, 681 (1946).

[20] J. M. Gérard, B. Sermage, B. Gayral, B. Legrand, E. Costard, and V. Thierry-Mieg, Phys. Rev. Lett. **81**, 1110 (1998).

[21] A. Fiore, U. Oesterle, R. P. Stanley, and M. Ilegems, IEEE Photonics Technol. Lett. **12**, 1601 (2000).

[22] A. Markus, A. Fiore, J. D. Ganière, U. Oesterle, J. X. Chen, B. Deveaud, M. Ilegems, and H. Riechert, Appl. Phys. Lett. **80**, 911 (2002).

[23] A. J. Bennett, P. N. Stavrinou, C. Roberts, R. Murray, G. Parry, and J. S. Roberts, J. Appl. Phys. **92**, 6215 (2002).

[24] K. Seeger, *Semiconductor Physics* (Springer-Verlag, Berlin, 1985).

[25] W. B. Joyce, J. Appl. Phys. **53**, 7235 (1982).

[26] S. Y. Hu, S. W. Corzine, K.-K. Law, D. B. Young, A. C. Gossard, L. A. Coldren, and J. L. Merz, J. Appl. Phys. **76**, 4479 (1994).

[27] G. J. Letal, J. G. Simmons, J. D. Evans, and G. P. Li, IEEE J. Quantum Electron. **34**, 512 (1998).

[28] J. K. Kim, T. A. Strand, R. L. Naone, and L. A. Coldren, Appl. Phys. Lett. **74**, 2752 (1999).

[29] D. P. Popescu, P. G. Eliseev, A. Stintz, and K. J. Malloy, J. Appl. Phys. **94**, 2454 (2003).

[30] A. Fiore, P. Borri, W. Langbein, J. M. Hvam, U. Oesterle, R. Houdré, R. P. Stanley, and M. Ilegems, Appl. Phys. Lett. **76**, 3430 (2000).

[31] V. Grillo, M. Albrecht, T. Remmele, H. P. Strunk, A. Y. Egorov, and H. Riechert, J. Appl. Phys. **90**, 3792 (2001).

[32] L. Grenouillet, C. Bru-Chevallier, G. Guillot, P. Gilet, P. Duvaut, C. Vannuffel, A. Million, and A. Chenevas-Paule, Appl. Phys. Lett. **76**, 2241 (2000).

[33] A. Polimeni, M. Capizzi, M. Geddo, M. Fischer, M. Reinhardt, and A. Forchel, Appl. Phys. Lett. **77**, 2870 (2000).

[34] R. A. Mair, J. Y. Lin, H. X. Jiang, E. D. Jones, A. A. Allerman, and S. R. Kurtz, Appl. Phys. Lett. **76**, 188 (2000).

[35] A. M. Mintairov, T. H. Kosel, J. L. Merz, P. A. Blagnov, A. S. Vlasov, V. M. Ustinov, and R. E. Cook, Phys. Rev. Lett. **87**, 277401 (2001).

[36] I. A. Buyanova, G. Pozina, P. N. Hai, N. Q. Thinh, J. P. Bergman, W. M. Chen, H. P. Xin, and C. W. Tu, Appl. Phys. Lett. **77**, 2325 (2000).

[37] L. Grenouillet, C. Bru-Chevallier, G. Guillot, P. Gilet, P. Ballet, P. Duvaut, G. Rolland, and A. Million, J. Appl. Phys. **91**, 5902 (2002).

[38] M. Albrecht, V. Grillo, T. Remmele, H. P. Strunk, A. Y. Egorov, G. Dumitras, H. Riechert, A. Kaschner, R. Heitz, and A. Hoffmann, Appl. Phys. Lett. **81**, 2719 (2002).

[39] A. Pomarico, M. Lomascolo, R. Cingolani, A. Y. Egorov, and H. Riechert, Semicond. Sci. Technol. **17**, 145 (2002).

[40] A. Hierro, J. M. Ulloa, J. M. Chauveau, A. Trampert, M. A. Pinault, E. Tournie, A. Guzman, J. L. Sanchez-Rojas, and E. Calleja, J. Appl. Phys. **94**, 2319 (2003).
[41] D. Fowler, O. Makarovsky, A. Patanè, L. Eaves, L. Geelhaar, and H. Riechert, Phys. Rev. B **69**, 153305 (2004).
[42] J. Teubert, P. J. Klar, W. Heimbrodt, K. Volz, W. Stolz, P. Thomas, G. Leibiger, and V. Gottschalch, Appl. Phys. Lett. **84**, 747 (2004).